Submission Template for IET Research Journal Papers

Sectorised Base Stations for FSO Ground to Train Communications

Nithin Mohan [1*], Mojtaba Mansour Abadi[1], Z. Ghassemlooy[1], S. Zvanovec[2], R. Hudson[3] and Manav R.Bhatnagar[4]

[1] Optical Communications Research Group, Faculty of Engineering and Environment, Northumbria University, Newcastle upon Tyne, UK
[2] Department of Electromagnetic Field, Faculty of Electrical Engineering, Czech Technical University in Prague, Czech Republic
[3] The Core, Bath Lane, Newcastle Helix, Newcastle upon Tyne
[4]Indian Institute of Technology Delhi, New Delhi 110016, India
[*]nithin.mohan@northumbria.ac.uk

Abstract: Evolution and accessibility of smart-phones have led to a huge demand in network bandwidth. The ubiquitous use of smart-phones in high-speed trains pose a unique challenge in delivering high-speed internet service on board. This challenge can be overcome by employing free space optics, an alternative to radio frequency technology. Previous coverage models for ground-train communications employed single laser systems with a larger divergence angle to cover a larger distance. Larger divergence angles lead to larger geometric losses, which may result in a non-reliable communication link. This paper proposes a sectorised multi-beam coverage model with a smaller divergence angle to reduce the impact of geometric losses in the system. This paper also proposes two receiver (Rx) architectures for Rxs deployed on the train. Along with geometric losses, the atmospheric attenuation is taken into consideration for the FSO link. The performance of the ground-train communications system in terms of bit-error-rate is evaluated under weak turbulence conditions via numerical simulation.

1. Introduction

With the increasing concerns regarding global warming, the governments and researchers are paying greater attention towards reducing greenhouse gas emission reduction, thus the Kyoto Protocol of 1997 [1]. Transport is one of the key contributors to past and future climate change. For global emissions, it has been shown that air travel has the highest specific climate impact (sCI), while rail and coaches have the lowest sCI [2]. Travelling by trains is the most environment-friendly, where the greenhouse effect of gas emissions per kilometre is 80% less than cars and they can carry more people and offer reduced noise pollution [3]. For rail transport to be even more attractive the passengers will demand access to broadband Internet access (BIA) for a range of applications including messaging, video on demand, voice over Internet protocol (VoIP), TV, streaming, videoconferencing, etc., where the train journey will be seen as the extension of working at home or office (i.e., the concept of home-to-office-to-home). In addition, broadband links between trains and infrastructure are essential for trains' safety and communications related information (i.e., trackside equipment, trains, signalling system, and people), which are needed by the network managers and railway operators.

In the past few years, we have seen a renewed interest in Internet connectivity on-board the trains, which are predominantly-based on radio frequency (RF) technologies. These are leaky coaxial cable (LCX), Wi-Fi and WiMAX with a maximum bandwidth of 2 Mbps, 54 Mbps and 40 Mbps, respectively, trackside and satellite [4]. The latter is better suited to certain types of traffic such as broadcast TV, where the bandwidth is shared across all the fleet and can improve the overall link performance by, for example, complementing the coverage offered by cellular systems. Alternatively, passengers could directly connect their smart devices via their cellular service provider to have BIA [5], [6], which requires sufficient radio coverage along the lines and suffers from RF signal attenuation (14 – 30 dB) due to Faraday cage [7]. One possible option to overcome this is to adopt relay-based systems at the cost of increased installation and maintenance costs. A train access terminal (TAT) or "mobile router" is another option to optimize performance and throughputs [8], which can support a number of many different technologies. In TAT, the incoming signal from the antenna positioned outside the train is fed to the access points in carriages, which overcome transmission losses and reduce the handover for all passengers into a single terminal with the aggregated traffic.

The average throughput for the aforementioned RF systems is at most 1.4 Mbps [4], which is unsatisfactory in terms of bandwidth required for web-conferencing (Skype call) and accessing video sharing sites (Netflix). This is mainly due to the availability of RF spectrum (i.e., the bandwidth) and multi-path propagation characteristics of the environment [9]. In accordance with UK Crosscountry Wi-Fi terms and conditions, any usage of service exceeding 70 Mb

in standard class and 100 Mb in the first-class coaches is classified as excessive usage and access to the Wi-Fi is reduced [10].

In [11], a mobile hot-spot network (MHN) was designed for subway trains using the millimetre-wave technology with a carrier frequency of 25.5 GHz. Two antennas or a mobile terminal equipment (MTE), which emit narrow beams, are installed at either end of the train. MTEs attempt to connect to MHN radio units deployed along the trackside and perform handover when the train crosses edges of the cells' coverage. The practical demonstration of MHN system yielded throughputs of 1.25 Gbps and 110 Mbps for the downlink and uplink, respectively [11]. In [12], a throughput of 1.5 Gbps using a 97 GHz millimetre wave radio access system connected via a bidirectional radio over fibre network for a train with the speed of up 240 km/h was experimentally demonstrated. The millimetre-wave distributed radio access units deployed on the ground were connected to the bidirectional analogue RoF network for establishing a high-speed link with the on-board transceiver. In [13], a 20 Gbps wavelength division multiplexed fibre-RF wireless system (at 90 GHz) between the central station and the base station (BS) was investigated within an indoor environment. The work in [13] is based on the moving BS concept where the high-speed train communicates with the same BS in order to prevent frequent handovers.

However, in the railway environment there are a number of issues that will affect wireless BIA on board the trains including: (*i*) Faraday cage – due to the metallic structure of the train, which results in power losses of transmitted signals; (*ii*) high vibration, which require isolation of communication devices; (*iii*) ground infrastructures; (*iv*) pylons, tunnels and overhead cables, which can result in loss of synchronization, disconnections, and packet losses; (*v*) adding/removing train carriages, where the communication networks need to detect this automatically; and (*vi*) the bandwidth bottleneck. The latter can be solved by employing free-space optical (FSO) wireless technologies. FSO offers a number of features including (i) huge unregulated license-free spectrum (i.e., bandwidth order of magnitude higher the RF technologies); (ii) excellent transmission security at the physical layer; (iii) robustness to the RF-induced electromagnetic interference; and (iv) compatibility with the backbone optical fibre networks [23].

Implementation of FSO for G2T communications focuses on providing a large coverage area for the BS, which reduces the deployment costs and provides uninterrupted internet service with negligible handover delay. Previous works on FSO systems have provided a comprehensive theoretical study and experimental validation on G2T communications. A high data rate (1 Gbps) G2T communications was proposed in [14], where an acquisition, tracking and pointing (ATP) mechanism based on the beaconing system was used to provide stable tracking and fast handover (i.e., 100 ms) in FSO links for high-speed trains. In [15], a high-speed image sensor based ATP mechanism was used in place of a 2-quadrant photodetector (PD) to detect the beacon signal from the adjacent BS. Using a new image processing algorithm for recognition and labelling beacon signals and a feedback control to control the direction of the mirror by employing a mirror angle sensor, the handover delay was reduced to 21 ms. In [16], rotating transceivers located on the ground and the train was employed to increase the coverage area. The rotating transceiver on the train switches from the source BS to a target BS, while the other transmitter (Tx) on the train maintains a continuous link from the source BS thereby mitigating the impact of handover. In [17], a dual transceiver scheme with a wide beam was proposed, which is deployed on both the ground and on the train, as opposed to a single rotating transceiver on the ground in [16], to increase the coverage area, reliability and the complexity of the FSO system. In [18], two FSO coverage models namely single wavelength and dual wavelengths were proposed for seamless handovers and high bandwidth communications.

The proposed system in [17] employs wide optical beams covering 250 m per transceiver with a divergence angle of 10 mrad to extend the trackside coverage, thereby reducing the number of FSO BSs. FSO links using wide divergence angle laser sources suffer from high geometric losses [20], which in case of wide beam systems may result in frequent link outages during handover between BS or result in frequent outages within the BS. In this paper, we propose a sectorised BS model for ground to train (G2T) communication, which provides a stable high-speed link between the train and the ground BSs under harsh weather conditions and mitigates the effect of geometric loss.

The rest of the paper is organized as follows. Section II describes ground-train communications which include G2T communications using sectorised BSs and train-to-ground (T2G) communications. Section III describes the system model. Results and discussion using numerical simulations pertaining to G2T communication are presented in section IV.

2. System Model

The system block diagrams for the intensity modulation/direct detection (IM/DD) FSO links for G2T and T2G communications are shown in Fig. 1. For G2T communications, see Fig. 1(a), the optical beam from the laser source is launched into a SMF the output of which is amplified using EDFA prior to being applied to a 1×10 fibre array. Lights from the fibre array are launched into a free space channel using diverging optics positioned at the end of each fibre. For T2G communications, see Fig. 1(b), 3 Txs (i.e., laser sources) with divergence angles of 60 mrad are used to illuminate the BSs. Optical beams propagating through the free space channel will experience both intensity and phase fluctuation due to the atmospheric fog and turbulence, which will degrade the link performance. For G2T and T2G communications, the received electrical signal is given by:

$$y = h(t) * x(t) + n(t), \quad (1)$$

where x is the transmitted signal, n is additive white Gaussian noise with variance σ_n^2 and h is the channel gain, which is given by:

$$h = h_a h_t h_g, \quad (2)$$

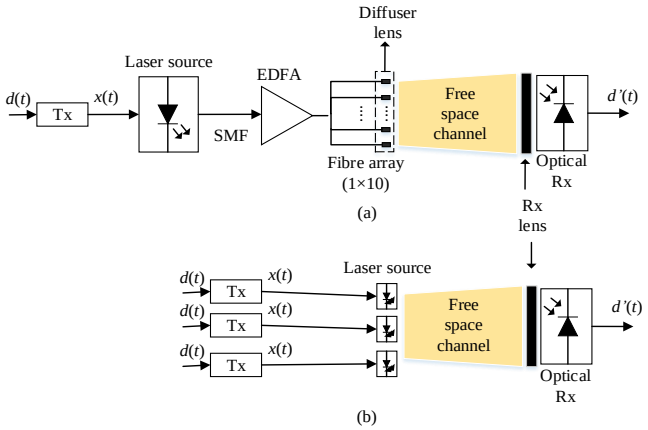

Fig. 1 A block diagram of line of sight FSO transmission for: (a) from ground-BS to the train and (b) from train to the ground-BS

h_a and h_t are attenuation constants due to the atmospheric channel and turbulence, respectively. For an FSO link, h_a is given by Beer's law [19]:

$$h_a = e^{-\beta l}, \tag{3}$$

where l is the link length in m and β is the attenuation coefficient in m^{-1}. The spreading of the propagating beam results in a spot size greater than the Rx's aperture, which leads to the geometric loss as given by [21]:

$$h_g = 10\log_{10}\left[\frac{d_{\mathrm{rx}}}{d_{\mathrm{tx}}+l_{link}\theta_{\mathrm{div}}}\right]^2, \tag{4}$$

where d_{tx} and $d_{\mathrm{rx}}$are the Tx and Rx's apertures, respectively and l_{link} is the link range. The optical intensity I of a wave propagating in turbulence channel undergoes random fading effect with the normalized variance or the scintillation index given as [22]:

$$\sigma_I^2 = \frac{\langle I^2\rangle-\langle I\rangle^2}{\langle I\rangle^2}, \tag{5}$$

where $\langle . \rangle$ denotes the ensemble average equivalent to long-time averaging with the assumption of an ergodic process. Based on (5), the strength of turbulence can be classified as weak ($\sigma_I^2 < 1$), moderate ($\sigma_I^2 \cong 1$) and strong ($\sigma_I^2 > 1$) [24]. Assuming plane wave propagation, σ_I^2 is given by [25]:

$$\sigma_I^2(D) = \exp\left[\frac{0.49\,\sigma_R^2}{\left(1+0.653d^2+1.11\sigma_R^{\frac{12}{5}}\right)^{\frac{7}{6}}}+\frac{0.51\,\sigma_R^2\left(1+0.69\,\sigma_R^{\frac{12}{5}}\right)^{-\frac{5}{6}}}{\left(1+0.9d^2+0.621\,d^2\sigma_R^2\right)^{\frac{12}{5}}}\right]-1, \tag{6}$$

Table 1 Key system parameters

Common Parameters	
Parameter	Value
Wavelength	1550 nm
Train speed	300 km/hr.
Tx and Rx apertures	1 and 20 cm
Track-BS distance	2 m
Rx power @17 dB	86.6 μW
Photodetector	PIN
Rx wavelength range	500-1630 nm
Rx 3 dB Bandwidth	10 kHz – 12 GHz
Noise equivalent power	24 pW/√*Hz*
Responsivity at 1550 nm	0.85 A/W

G2T Communications				
Fiber number	Tilt angle (δ) (mrad)	Transmit power (mW)	Beam divergence (mrad)	Coverage length (m)
1, 10	24	43.0	5	20
2, 9	31	57.2	8	20
3, 8	45	62.7	15	20
4, 7	66.5	68.6	24	15
5, 6	100	72.0	37.5	10

Receiver Lens G2T communications	
Diameter	200 mm
Effective focal length	400 mm
Wavelength	350-2200 nm

EDFA	
Operating wavelength	1535-1563 nm
Output power (@ 0 dBm input power)	> +30 dBm
Noise figure	< 4.3 dB

Receiver Lens T2G communications	
Diameter	250 mm
Effective focal length	400 mm
Wavelength	350-2200 nm

where $d = \frac{D}{2}\sqrt{\frac{k}{l}}$ is the circular aperture scaled by Fresnel zone provided, k is the wavenumber and D is the Rx's aperture diameter. σ_R^2 is Rytov variance given by:

$$\sigma_R^2 = 1.23C_n^2k^{7/6}l^{11/6}, \tag{7}$$

where C_n^2 is the refractive index structure constant with typical values of 10^{-17} $m^{-2/3}$ and 10^{-13} $m^{-2/3}$ for weak and strong turbulence regimes, respectively [22]. Log-normal distribution serves as a good approximation for turbulence regimes where $\sigma_I^2 < 0.3$ [24] and the average bit-error-rate (BER) for log-normal turbulence is approximately given by [26]:

$$P_e \approx \frac{1}{\sqrt{\pi}}\sum_{i=1}^{g} w_i Q\left(\frac{\eta I_0 e^{-2\sigma_x^2+z_i\sqrt{8\sigma_x^2}}}{\sqrt{2N_0}}\right), \tag{8}$$

where, g is the order of approximation, z_i, i = 1,…, g is the zero of the g^{th} order Hermite polynomial, w_i is the weight factor for the g^{th}-order approximation, I_0 is the signal light intensity without turbulence, $\sigma_x^2 \approx \sigma_I^2/4$ is the variance of log-amplitude fluctuations, η is the optical-to-electrical

conversion coefficient and N_0 is the noise power spectral density.

A) *Power budget analysis*

The received power can be expressed as a function of the transmit power P_{tx} and the system losses is given by:

$$\mathrm{P_{rx}}(l) = 10^{\frac{(L_{\text{atm}}l)}{10}} \times 10^{\left(\frac{h_g}{10}\right)} \times 10^{\left(\frac{L_{\text{Misc}}}{10}\right)} P_{\text{tx}} \quad (9)$$

where L_{atm} is given by [18]:

$$L_{\text{atm}} = \frac{17}{V}\left(\frac{\lambda}{550}\right)^{-q}, \quad (10)$$

where V is the meteorological visibility in km, λ is the wavelength in nm and q is the size distribution of scattering particles, which follows Kruse [20] model and is expressed as:

$$q = \begin{cases} 1.6 & V > 50 \text{ km} \\ 1.3 & 6 \text{ km} < V < 50 \text{ km} \\ 0.16V + 34 & 1 \text{ km} < V < 6 \text{ km} \\ V - 0.5 & 0.5 \text{ km} < V < 1 \text{ km} \\ 0 & V < 0.5 \text{ km} \end{cases} \quad (11)$$

L_{Misc} is the coupling losses due to optics to fibre and fibre to coupling. For a Gaussian beam, the received optical power at any point along the rail track is given by the beam offset r and its radius w_R as shown in Fig. 3 [18], is given as [16, 18]:

$$\frac{P_{\text{rx}}(r,l)}{P_{\text{rx}}(l)} = e^{-\frac{2r^2}{w_R^2}}. \quad (12)$$

Combining (9) and (12), the received power can be expressed as:

$$P_{\text{rx}}(r,l) = 10^{\frac{(L_{\text{atm}}l)}{10}} \times 10^{\left(\frac{h_g}{10}\right)} \times 10^{\left(\frac{L_{\text{Misc}}}{10}\right)} \times e^{-\frac{2r^2}{w_R^2}}. \quad (13)$$

3. Ground to Train Duplex Communications

G2T duplex communications system is analysed based on the parameters provided in Table 1. The parameters shown in Table 1 were obtained based on the signal model presented in section II and the following criteria of (*i*) h_g limited to 15 dB per beam; and (*ii*) a minimum train (i.e., track) coverage length of 10 m per beam. Fig. 2 shows the schematic block diagram of G2T system based on a sectorised BS, which uses a laser/fibre array for illumination of the train (i.e., trackside) in order to provide a data communications link. A single laser source is used the output of which is amplified using an erbium-doped fibre amplifier (EDFA) prior to being split into 10 fibre-based Txs. Beam expanding optics are used to expand the light emerging from the fibre-array for illuminating moving train. Note, the spacings between the beam expanders are 7 cm, and the overlapping areas of the optical beams on the track are 2 m in order to provide seamless connectivity throughout the coverage length of 210 m (i.e., the spacing between BSs). As illustrated in Fig. 2, the effective coverage length along the track is 170 m (i.e., 2×85 m) and there is a dead-zone of 40 m where there is no need for optical illumination. Note, in FSO links a single beam with a large divergence angle can effectively cover a wide area but at the cost of increased h_g, which ultimately limits the transmission range and thus the maximum achievable transmission data rates. Though the h_g can be mitigated by increasing the transmit power, however, the eye and skin safety regulation will set the maximum transmit optical power level. In this work, we have adopted the sectorised BS topology with reduced the divergence angle per optical Tx.

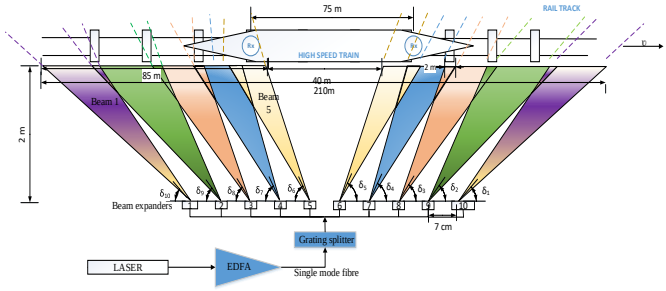

Fig. 2 The laser/fibre array covers 170 m (85 m on either side). The distance between the two BSs is 210 m.

Based on the experimental work conducted on a commuter train travelling at a speed of 130 km/h the physical layer handover delay was reported to be 120 ms [27]. Using a handover delay time of 120 ms as the benchmark, the separation between the two Rxs on the train should be 75 m, see Fig. 3. This allows allocation of a delay time of 210 ms for the inter-BS and intra-BS handover for each Rx for a train travelling at a speed of 300 km/hr while the other Rx is still in communications with the ground BS to ensure seamless connectivity. In [27], a tracking scheme was proposed where the delay in the physical layer was contributed due to the physical mirror handover time. The Rxs on the train are composed of a lens and an optical Rx (i.e., a PD and a trans-impedance amplifier). The regenerated electrical signal is applied to a matched filter and then to a threshold detector (slicer) in order to recover the transmitted data stream.

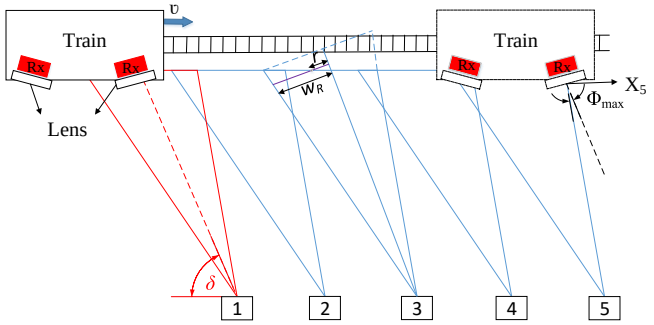

Fig. 3 The Rx's alignment offset angle with respect to the transmit beam (1-5) direction.

As shown in Fig. 3, the Rx's are aligned with beam 1, where δ is the tilt angle of the beam 1. With the train travelling from left to right, the Rx will have an offset angle Φ_{max} with respect to the beam directions, see Fig. 3, which is given by:

$$\Phi_{max} = \tan^{-1}\left(\frac{x_{\text{track}}}{y_d}\right) - \delta, \quad (14)$$

For the T2G link, three Txs are located on the roof of the train one at each ends with a spacing of d pointing to the BSs as depicted in Fig. 4, which provides a seamless handover between the BSs. The transmitted beams with the

divergence angle of θ illuminate the track side (i.e., the BSs) with coverage length of x and with some beam overlapping. In order for the train to establish a connection with the next BSs prior to dropping the connection with current BS, the coverage length is made to be larger than the spacing between two BSs, see Fig. 4.

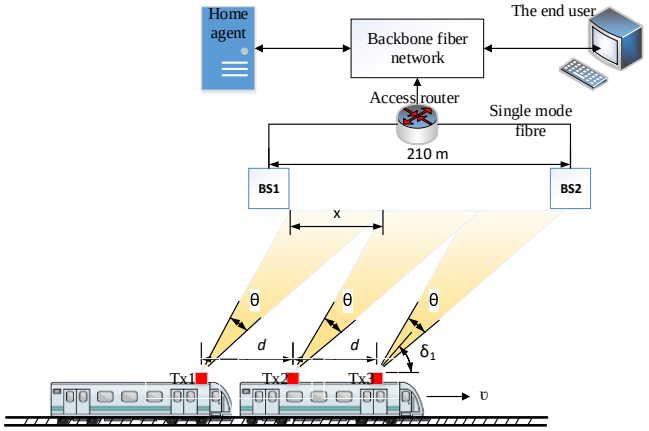

Fig. 4 Train to ground communication where the coverage area of each transceiver is 75m. The transceivers are spaced 75m apart from each other.

Note, at the Rx a lens is used to focus the beam onto a small area PD or an optical fibre pigtailed optical Rx. However, for a moving train, the lens focal point position is no longer stationary and is moving away from the centre position (i.e., when the train is stationary), see Fig. 5, which results in the loss of beam being coupling to the optical Rx (i.e., link failure). Therefore, the vertical offset of the lens focal point is given as:

$$\Delta q = f \times \tan \Phi, \tag{15}$$

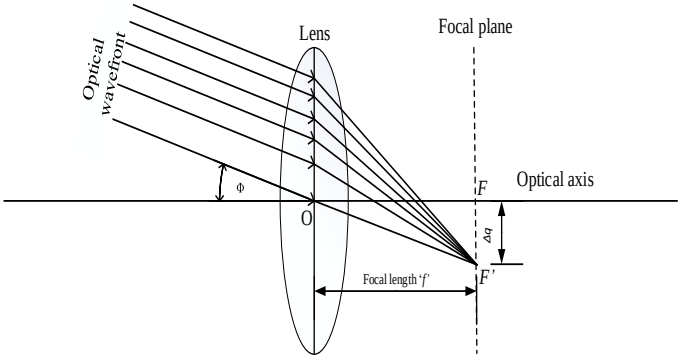

Fig. 5 Oblique beam through a perfect lens

where f is the focal length. For Φ and f of 4.431° and 40 cm, respectively the maximum Δq is 3 cm**,** which is orders of magnitude larger than the surface area of a high-speed PD (e.g., 60 μm). To overcome this problem and ensure light coupling there are a number of possible solutions including (*i*) Rx diversity, which is highly costly and complex; (*ii*) tracking Rx; (*iii*) fibre-based coupling; and (*iv*) cascading lenses. In this work, (*iii*) and (*iv*), which are simpler to implement, are adopted. Fig. 6 shows an Rx arrangement based on the cascading lenses, where the incoming light following propagation through lenses is coupled into a multimode fibre (MMF) array, which is positioned at the radial gradient (curve) of the cascading lenses focal points. The emerging light beams from the MMF array is coupled into a series of PDs using a collimator and a photonic lantern. By using equal gain combining (EGC), all the PD's currents can be summed and processed as whole. The equivalent focal length f_{eq} for n lenses is given by:

$$\frac{1}{f_{\text{eq}}} = \frac{1}{f_1} + \frac{1}{f_2} + \cdots . + \frac{1}{f_n} \tag{16}$$

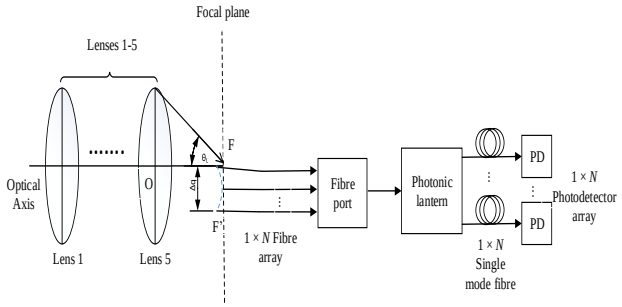

Fig. 6 The Rx configuration based on series of cascading lenses

Fig. 7 depicts the vertical displacement with respect to Φ for f of 40 cm, which represents a single lens setup and 8 cm, for five cascaded lens setup. The variation of Δq is in orders of millimetres for reduced f. Note that, light passing through an uncoated glass substrate undergoes Fresnel reflection, thus resulting in ~ 8% light reflection at each interface. Due to this effect, only 92% of the incoming light is transmitted through each lens, thus only 65% of the incident light is emerging from lens 5. One possible solution would be to apply anti-reflection coating on each lens thereby increasing the optical transmission. For light coupling into a fibre, the incident angle of the light from the lens should be less than the numerical aperture (NA) of MMF, which is given by:

$$\theta_L = \tan^{-1}\left(\frac{0.5D_L}{f}\right), \tag{17}$$

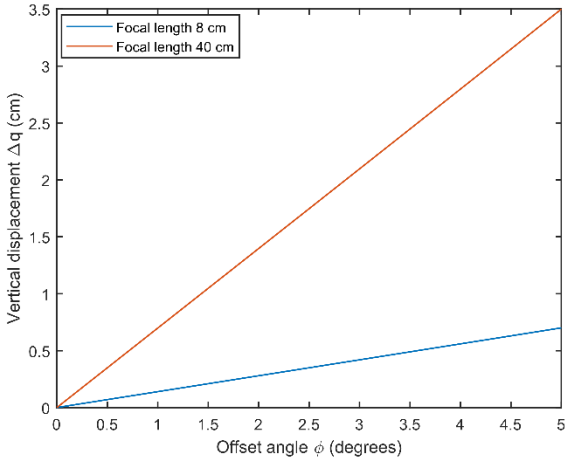

Fig. 7 Vertical displacement as a function of the offset angle for f of 8 and 40 cm.

where D_L is the lens diameter. For f of 8 cm and a lens diameter of 20 cm, θ_L will be 51.34°. The commercially available MMF has a maximum NA of 0.5, which

corresponds to an acceptance angle of 30°, which is smaller than θ_L thus resulting in large coupling losses.

Fig. 8 shows fibre-based coupling Rx arrangement where the incoming light from the lens is coupled directly onto the multi-mode fibre array placed along the focal plane of the lens. Light from the MMF array is coupled into the PDs using a collimator and a photonic lantern. The EGC technique is used for signal processing. Note that, Δq is large and would require more fibres for coupling light compared with the cascading lens, see Fig. 6.

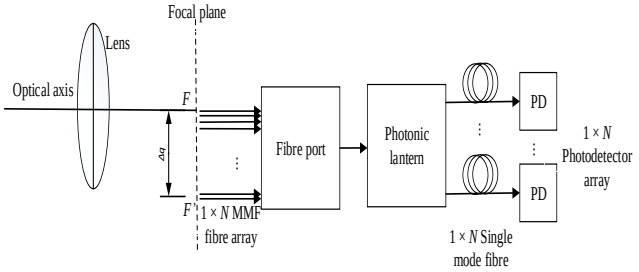

Fig. 8 Schematic block diagram of a single lens setup

4. Results and Discussion

The proposed systems are numerically simulated using the parameters given in Table 1. Fig. 9 depicts the geometric loss h_g as a function of the transmission distance between the BS and the train for the first five fibre-based Txs as shown in Fig. 2. From Fig. 9 it is observed that, h_g is the lowest and highest for the fibres 5 and 1, respectively with the attenuation difference of ~6 dB. Note, beams 1 and 5 have the lowest and highest divergence angles of 5 and 37.5 mrad, Using (13) and the parameters shown in Table 1, the transmit power for each beam as a function of transmission range for the G2T under the fog condition with a visibility of 0.5 km is depicted in Fig. 10. The coupling losses between the lens and MMF is assumed to be 2 dB. It is assumed that the photonic lantern has a bundle of seven single mode fibres [29] connected to the PDs. The average multimode to single mode loss per fibre is 0.56 dB, which gives a total loss of ~4 dB for seven fibres. Therefore, the total loss for L_{Misc} is 6 dB. As shown in Fig. 10 the beams display minimum transmit power levels of 9.2, 9.69, 9.182, 5.6 and 4.3 mW are for Txs 1 to 5, at the transmission distances of 25, 37.5, 55, 75 and 95 m, respectively. The intersections on each beam depict the 2 m overlap between two beams as shown in Fig 1(a).

To mitigate the losses exhibited by the system, the maximum transmit power of each beam is considered as the transmit power required by each beam as shown in Table 1. Using commercially available beam splitters the optical power distributions for each fibre for the G2T communications are shown in Table 2. Note that, for an input power of 0 dBm at the EDFA the output power is 30 dBm, which corresponds to 1W. The total power required for fibres 1-5 is calculated to be 360 mW from Table 2. Similarly, for fibres 6-10, the optical power would be 360 mW. The cumulative power requirement for each BS is 606.8 mW, which is within the EDFA power limit.

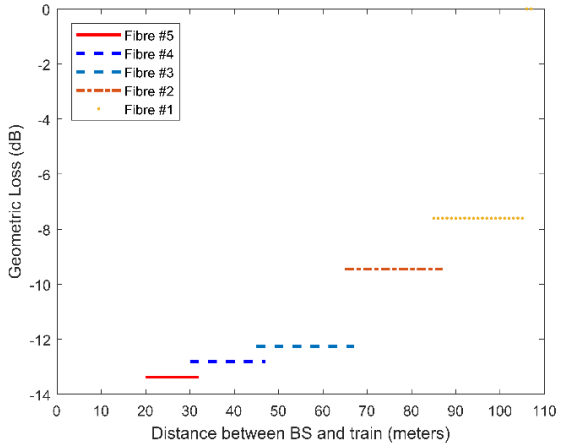

Fig. 9 The geometric loss versus the transmission distance for laser/fibre 1-5

The maximum geometric loss is contributed by fibres 1 and 10, which is -13.38 as depicted in Fig. 9. The average geometric loss contributed by fibres 1-5 is 11.10 dB. In contrast with single beam systems, the geometric loss is double the average geometric loss encountered by the sectorised BS approach as given in Table 3. As a result, the transmit power/laser for a single beam-based system with a coverage length of 55 m is more than twice that of the sectorised BS approach.

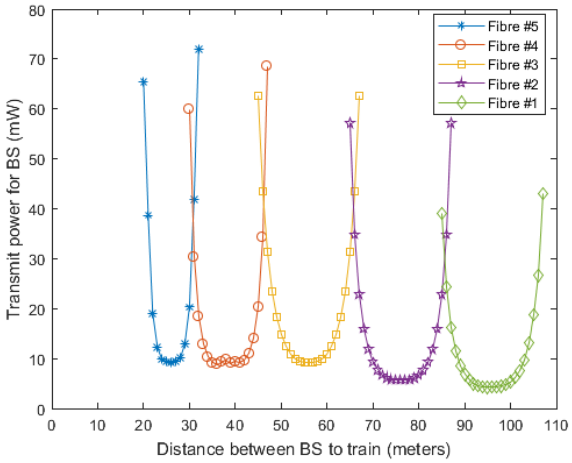

Fig. 10 The transmit power as a function of transmission distance for laser/fibre 1-5

For moderate to strong turbulence the Gamma-Gamma turbulence model is considered to be a good fit for irradiance fluctuations encountered by the Rx's aperture [28].

Table 2 Power distribution for each fibre using commercially available splitters

TRANSMIT POWER				
Fiber number	Tilt angle (δ) (mrad)	Transmit power (mW)	Beam divergence (mrad)	Coverage length (m)
1, 10	24	54	5	20
2, 9	31	63	8	20
3, 8	45	63	15	20
4, 7	66.5	90	24	15
5, 6	100	90	37.5	10
BEAM SPLITTERS				
Splitting ratio		30:70 and 50:50		

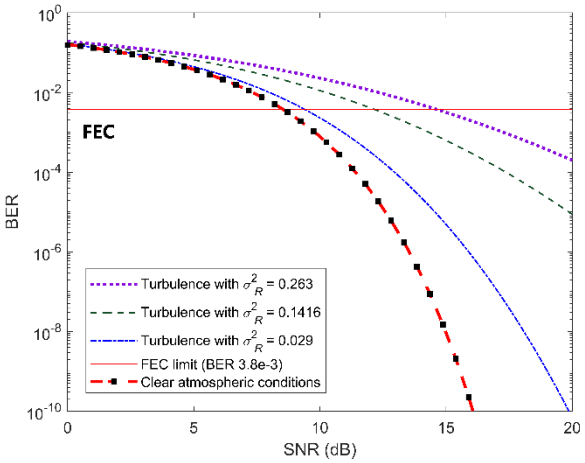

Fig. 11 Average BER as a function of SNR for σ_R^2 of 0.263, 0.1416 and 0.029

For a point Rx (D = 0), $C_n^2 = 9 \times 10^{-13}$ m$^{-2/3}$ and a maximum link distance l_{link} of 100 m, the scintillation index is calculated to be 3.12 from (6), which categorises the turbulence to be moderate to strong turbulence. Since the Rx in this case averages the fluctuations resulting in reduced scintillation as compared to a point Rx, therefore the G2T link is considered as a lognormal fading channel. Using (8) simulations were carried to determine the BER performance of the link for weak turbulence range of σ_R^2 = 0.263 and $C_n^2 = 9 \times 10^{-13}$ m$^{-2/3}$, σ_R^2 = 0.1416 and $C_n^2 = 5 \times 10^{-13}$ m$^{-2/3}$ and σ_R^2 = 0.029 and $C_n^2 = 1 \times 10^{-13}$ m$^{-2/3}$ for the OOK-NRZ modulation format is depicted in Fig. 11. It is observed that, for all these cases the BER is below the FEC limit. The BER can be significantly improved by incorporating forward error correcting coding techniques [25].

Table 3 Transmit power and geometric loss incurred for single beam systems

SINGLE BEAM SYSTEMS				
Coverage length per laser	Tilt angle (δ) (mrad)	Beam divergence (mrad)	Geometric loss (dB)	Transmit power (mW)
85	59.4	80.6	-22.7	1063
75	60.4	78.6	-22.3	964
65	61.6	76.1	-22.0	904
55	63.2	73.0	-21.4	783

Table 4 provides a comparison between the proposed system architecture and others reported in the litrature.

Table 4 Comparison between different system architectures

System Architecture	Transmission data rate (Gbps)	Transmission wavelength (nm)	Distance between successive base stations (m)
RATE [16]	0.1	850	415
DRIVE [17]	1	850	887
Dual wavelength model [18]	1.25	850 and 1550	222
The proposed work	**10**	**1550**	**210**

5. Conclusion

In this paper, a sectorised multi-laser coverage system was proposed in order to mitigate the geometric loss experienced by single beam systems. The paper describes duplex communication between the train and the BS. Power budget analysis was carried out under heavy fog conditions to determine the transmit power required for each fibre at the BS and at the transmitter deployed on the train. As the ground-train communication system employs large apertures at the Rx, the fluctuations are averaged over the Rx resulting in reduced scintillation as compared to a point Rx. Due to the effect of aperture averaging, our analysis considers log-normal distribution as a good approximation for weak to strong turbulence regimes. Numerical simulations were carried out to determine the ground-train communications performance under turbulence of varying strength. In all cases, the system BER was found to be below the FEC limit. At the FEC limit. the SNR penalties observed for σ_R^2 = 0.263, 0.1416 and 0.029 are 0.7, 3.28, 5.83 dB, respectively. This paper also proposes two Rx architectures for the deployment on the train.

6. Acknowledgments

This work is supported by intensive industrial innovation program northeast, United Kingdom (IIIP NE) - 25R17P01847 and is partly funded by the European regional development fund (ERDF).

7. References

[1] United Nations Framework Convention on Climate Change (UNFCCC), 1998. Kyoto protocol to the United Nations framework convention on climate change. http://unfccc.int/essential_background/kyoto_protocol/items/1678.php (accessed June 2019).

[2] Borken-Kleefeld, J., Berntsen, T., Fuglestvedt, J., 2010. Specific climate impact of passenger and freight transport. Environmental Science & Technology 44, 5700–5706.

[3] https://www.saveatrain.com/blog/why-choosing-to-travel-by-train-is-environmentally-friendly/, accssed June 2019

[4] M. Terada and F. Teraoka, "Providing a high-speed train with a broadband and fault tolerant IPv4/6 NEMO environment," 2012 IEEE Globecom Workshops, Anaheim, CA, 2012, pp. 1052-1056.

[5] L. Verstrepen et al., "Making a well-founded choice of the wireless technology for train-to-wayside data services," 2010 9th Conference of Telecommunication, Media and Internet, Ghent, 2010, pp. 1-7.

[6] M. K. Müller, M. Taranetz and M. Rupp, "Providing current and future cellular services to high speed trains," in IEEE Communications Magazine, vol. 53, no. 10, pp. 96-101, October 2015.

[7] Y. Zhou, Z. Pan, J. Hu, J. Shi and X. Mo, "Broadband wireless communications on high speed trains," 2011 20th Annual Wireless and Optical Communications Conference (WOCC), Newark, NJ, 2011, pp. 1-6.

[8] ACCORDE. (2008) ACORDE - Broadband Railway Internet Access on High Speed Trains Via Satellite Links. Press release. Accorde. Santander, Spain. [Online]. Available: http://www.railway-technology.com/contractors/signal/acorde/

[9] R. Paudel, X. Tang and Z. Ghassemlooy, "Laboratory demonstration of FSO ground-to-train communications with multiple base stations," 2016 10th International Symposium on Communication Systems, Networks and Digital Signal Processing (CSNDSP), Prague, 2016, pp. 1-6.

[10] Welcome to CrossCountry. (2019). Retrieved from https://www.crosscountrytrains.co.uk/on-board-with-crosscountry/wifi-on-board

[11] H. Chung et al., "From architecture to field trial: A millimeter wave based MHN system for HST Communications toward 5G," 2017 European Conference on Networks and Communications (EuCNC), Oulu, 2017, pp. 1-5.

[12] A. Kanno et al., "Field Trial of 1.5-Gbps 97-GHz Train Communication System Based on Linear Cell Radio Over Fiber Network for 240-km/h High-Speed Train," 2019 Optical Fiber Communications Conference and Exhibition (OFC), San Diego, CA, USA, 2019, pp. 1-3.

[13] P. T. Dat, A. Kanno, K. Inagaki, F. Rottenberg, N. Yamamoto and T. Kawanishi, "High-Speed and Uninterrupted Communication for High-Speed Trains by Ultrafast WDM Fiber–Wireless Backhaul System," in Journal of Lightwave Technology, vol. 37, no. 1, pp. 205-217, 1 Jan.1, 2019

[14] H. Urabe et al., "High Data Rate Ground-to-Train FreeSpace Optical Communication System," Optical Engineering, Special Section on Free-Space Laser Communications, vol. 51, no. 3, Mar. 2012.

[15] K. Mori et al., "Fast handover mechanism for high data rate ground-to-train free-space optical communication system," 2014 IEEE Globecom Workshops (GC Wkshps), Austin, TX, 2014, pp. 499-504.

[16] Q. Fan, M. Taheri, N. Ansari, J. Feng, R. Rojas-Cessa, M. Zhou and T. Zhang, "Reducing the Impact of Handovers in Ground-to-Train Free Space Optical Communications," in IEEE Transactions on Vehicular Technology, vol. 67, no. 2, pp. 1292-1301, Feb. 2018.

[17] Q. Fan, N. Ansari, J. Feng, R. Rojas-Cessa, M. Zhou and T. Zhang, "Reducing the Number of FSO Base Stations With Dual Transceivers for Next-Generation Ground-to-Train Communications," in IEEE Transactions on Vehicular Technology, vol. 67, no. 11, pp. 11143-11153, Nov. 2018.

[18] S. Fathi-Kazerooni et al., "Optimal Positioning of Ground Base Stations in Free-Space Optical Communications for High-Speed Trains," in IEEE Transactions on Intelligent Transportation Systems, vol. 19, no. 6, pp. 1940-1949, June 2018.

[19] . E. Leitgeb, S. S. Muhammad, C. Chlestil, M. Gebhart and U. Birnbacher, "Reliability of FSO links in next generation optical networks," Proceedings of 2005 7th International Conference Transparent Optical Networks, 2005., Barcelona, Catalonia, 2005, pp. 394-401 Vol. 1.

[20] P. W. Kruse, L. D. McGlauchlin, and R. B. McQuistan, Elements of Infrared Technology: Generation, Transmission, and Detection. New York, NY, USA: Wiley, 1962

[21] Scott Bloom, Eric Korevaar, John Schuster, and Heinz Willebrand, "Understanding the performance of free-space optics [Invited]," J. Opt. Netw.2, 178-200, 2003.

[22] S. Rajbhandari, Z. Ghassemlooy, P. A. Haigh, T. Kanesan and X. Tang, "Experimental Error Performance of Modulation Schemes Under a Controlled Laboratory Turbulence FSO Channel," in Journal of Lightwave Technology, vol. 33, no. 1, pp. 244-250, 1 Jan.1, 2015.

[23] Ieee802.org, 2019. [Online]. Available: http://ieee802.org/3/10G_study/public/july99/azadet_1_0799.pdf. [Accessed: 02- Jul- 2019].

[24] M. M. Abadi, Z. Ghassemlooy, N. Mohan, S. Zvanovec, M. R. Bhatnagar and R. Hudson, "Implementation and Evaluation of a Gigabit Ethernet FSO Link for 'The Last Metre and Last Mile Access Network'," 2019 IEEE International Conference on Communications Workshops (ICC Workshops), Shanghai, China, 2019, pp. 1-6.

[25] M. A. Khalighi, N. Aitamer, N. Schwartz and S. Bourennane, "Turbulence mitigation by aperture averaging in wireless optical systems," 2009 10th International Conference on Telecommunications, Zagreb, 2009, pp. 59-66.

[26] S. M. Navidpour, M. Uysal and M. Kavehrad, "BER Performance of Free-Space Optical Transmission with Spatial Diversity," in IEEE Transactions on Wireless Communications, vol. 6, no. 8, pp. 2813-2819, August 2007.

[27] H. Urabe, S. Haruyama, T. Shogenji, S. Ishikawa, M. Hiruta, F. Teraoka, T. Arita, H. Matsubara, and S. Nakagawa, "High Data Rate Ground-to-Train Free-Space Optical Communication System," Optical Engineering, vol. 51, no. 3, pp. 031 204–1–031 204–9, March 2012.

[28] A. Prokeš, "Modeling of atmospheric turbulence effect on terrestrial FSO link," Radioengineering, vol. 18, no. 1, pp. 42–47, Jan. 2009.

[29] D. Noordegraaf, P. Skovgaard, M. Nielsen and J. Bland-Hawthorn, "Efficient multi-mode to single-mode coupling in a photonic lantern", *Optics Express*, vol. 17, no. 3, p. 1988, 2009. Available: 10.1364/oe.17.001988.